Multiphoton-Absorption-Excited Up-Conversion Luminescence in Optical Fibers

Fabio Mangini,[1,†] Mario Ferraro,[2,*,†] Mario Zitelli,[2] Alioune Niang,[1] Alessandro Tonello,[3] Vincent Couderc,[3] and Stefan Wabnitz[2,4]

[1] *Department of Information Engineering, University of Brescia, Via Branze 38, 25123 Brescia, Italy*
[2] *Department of Information Engineering, Electronics, and Telecommunications, Sapienza University of Rome, Via Eudossiana 18, 00184 Rome, Italy*
[3] *Université de Limoges, XLIM, UMR CNRS 7252, 123 Avenue A. Thomas, 87060 Limoges, France*
[4] *Novosibirsk State University, Pirogova 1, Novosibirsk 630090, Russia*

(Received 26 August 2020; revised 25 October 2020; accepted 27 October 2020; published 24 November 2020)

We experimentally demonstrate a previously unforeseen nonlinear effect in optical fibers: up-conversion luminescence generation excited by multiphoton absorption of femtosecond infrared pulses. We directly estimate the average number of photons involved in the up-conversion process, by varying the wavelength of the pump source. We highlight the role of nonbridging oxygen hole centers and oxygen-deficient center defects and directly compare the intensity of side-scattered luminescence with numerical simulations of pulse propagation.

DOI: 10.1103/PhysRevApplied.14.054063

I. INTRODUCTION

Up-conversion luminescence (UL), involving the absorption of multiple photons followed by the emission of higher-energy photons via the radiative decay of excited electron energy levels in dielectric materials, has attracted considerable research attention since its first observation in rare-earth-doped crystals [1]. Over the years, UL has found application in a wide range of fields, moving from physics to chemistry and biology, since it allows for the detection of several stimuli such as temperature, electromagnetic radiation, and *p*H [2]. Due to developments in materials nanoengineering, UL has been recently proposed for medical therapy too [3]. In physics, UL finds its main application in the generation of visible laser emission by means of infrared optical pumping [4,5].

With the aim of realizing fiber lasers, various authors have studied UL in optical fibers, doped with different types of semiconductors, such as cesium, europium, and tantalum [6–8]. In their first report of UL in silica glass, which is the main constituent of commercial optical fibers, Kazansky *et al.* attributed their observation of multiphoton-absorption- (MPA) excited up-conversion luminescence in Ge-doped silica glass to the presence of Ge–oxygen-deficient center (Ge-ODC) defects [9]. However, intrinsic and induced defects in silica had already been studied by using ultraviolet- (UV) pumped visible photoluminescence. Among these, the presence of the so-called nonbridging-oxygen-hole-center (NBOHC) defects, responsible for visible-red-light emission at 650 nm, has attracted significant interest [10]. NBOHCs consist of a complementary pair of broken silicon-oxygen bonds and have been among the first defects to be studied. Their paramagnetic properties permit one to investigate NBOHCs by means of the electron paramagnetic resonance technique. Only later was the presence of diamagnetic defects, such as Ge-ODCs, also discovered in silica glass [11]. These defects are responsible for several luminescence bands in the UV-VIS spectral range. Three main emission bands, centered at 290, 400, and 460 nm, have been easily detected in as-grown or irradiated silica [12,13], as well as in Ge-doped silica [14]. Ge-ODC luminescence has also been observed in single-mode optical fibers [15] and it has been proposed as an alignment marker for the manufacturing of fiber Bragg gratings [16]. Luminescence from defects and impurities represents a useful tool for the spectroscopy of transparent media and permits one to extend the range of laser emission into the UV. Luminescence has recently been proposed as a tool for supercontinuum generation in yttrium-aluminum-garnet (YAG) crystals [17]. In optical fibers, UL provides an interesting means by which to extend the supercontinuum bandwidth into the UV, which is otherwise challenging if using parametric nonlinear effects [18,19].

In this paper, we report the experimental observation and theoretical description of visible UL in commercial multimode fibers (MMFs), pumped by intense femtosecond infrared laser pulses. Owing to their large numerical

*mario.ferraro@uniroma1.it
†These authors contributed equally to this work.

aperture, MMFs are better suited than single-mode fibers to trap luminescent radiation. Moreover, because of their relatively large core size, MMFs may carry light beams with peak powers up to the self-focusing critical value, before any permanent damage occurs. This allows for the observation of a host of unexpected nonlinear effects [18,20]. Specifically, the presence of photoluminescence and nonlinear losses, which have been ascribed to a MPA mechanism, has recently been reported in graded-index (GRIN) MMFs [21,22]. These nonlinear losses introduce a fundamental nonlinear limitation to the energy transmission capabilities of optical fibers and may provide an intrinsic limitation for the power scaling of spatiotemporal mode locking with multimode fiber lasers [23].

To date, a microscopic interpretation of these intriguing phenomena is still lacking. Here, we fill this gap in the knowledge, by associating them with UL. Specifically, we unveil a previously unforeseen nonlinear phenomenon in optical fibers, by demonstrating the presence of the up-to-five-photon absorption processes involved in UL generation. Spatial self-imaging (SSI) in GRIN fibers plays a key role in enhancing UL, which becomes visible to the naked eye as an array of side-scattering blue emitters. Our experimental results are in excellent quantitative agreement with numerical simulations based on a generalized nonlinear Schrödinger equation (GNLS). We provide a complete characterization of the multiphoton nature of UL, by varying the laser power and wavelength, and compare UL spectra for GRIN and step-index MMFs.

II. METHODS

In our experiments, we measure the spectrum of visible UL light scattered out of the first few millimeters of propagation in MMFs. This light results from the multiphoton absorption of high-peak-power (up to 3-MW) femtosecond infrared pulses. Spectra are collected using a miniature fiber optics spectrometer (Avaspec-2048). As a pump source, we use a hybrid optical parametric amplifier (OPA) pumped by a femtosecond Yb-based laser. Pulses of 80 fs at 650–940 nm (from the OPA) or 180 fs at 1030 nm (from the pump laser directly) with a 100 kHz repetition rate are coupled into two different multimode standard fibers: a 50/125 GRIN fiber with a relative index difference $\Delta_{\mathrm{GRIN}} = 0.0103$, and a 105/125 step-index fiber with $\Delta_{\mathrm{SI}} = 0.012$. In both cases, the beam $(1/e^2)$ diameter at the fiber input facet is equal to 7.55 μm at $\lambda = 1030$ nm and about 11 μm at $\lambda = 650$–940 nm. The UL is collected by means of an imaging lens into either the spectrometer or a microscope.

In Fig. 1(a) we present a sketch of our setup. Figure 1(b) shows images of the side-scattered UL spots, taken using a Dinolite-AM3113T digital microscope. The different scattering patterns from either the GRIN or the step-index fibers can be clearly appreciated. A single emission spot

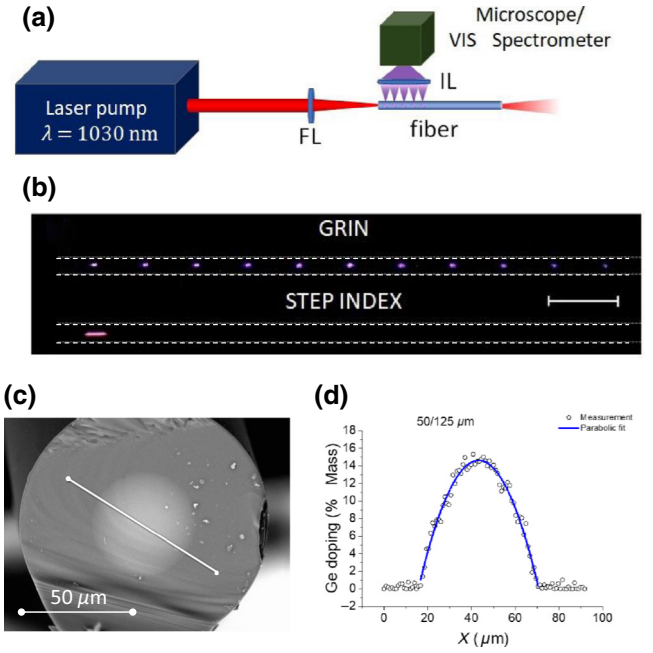

FIG. 1. (a) A schematic of the experimental setup. (b) A microscope image of the luminescence scattered from either the GRIN or the step-index fibers. The dashed lines denote the cladding-air interface, while the scale bar corresponds to 1 mm. (c) A SEM image of a GRIN fiber section. (d) The %-mass Ge concentration in the Ge-doped GRIN fiber.

at the point of minimum beam waist is scattered from the step-index fiber, whereas the periodic beam focusing in the GRIN fiber leads to an array of scattering points. The two fibers also differ in terms of their dopants and concentrations. Specifically, in the step-index fiber, the cladding is made of fluorine-doped silica, while the core is nominally undoped. In contrast, index grading in the GRIN fiber is obtained by using a parabolically decreasing concentration of Ge dopant in the core and the cladding is made of pure silica. In Fig. 1(c), a scanning-electron-microscope (SEM) image of the GRIN-fiber facet is reported. We spatially track the Ge concentration along a diameter of the core (white line in the figure) by means of energy-dispersive x-ray spectroscopy (EDX), which provides a well-known signature in the electromagnetic spectrum. The result is shown in Fig. 1(d). At its peak, the Ge-doping is 15% mass (corresponding to 4.5% atomic).

III. RESULTS

In Fig. 2(a), we illustrate the dependence of the measured intensity spectrum of the side-scattered light on the peak power (P_p) of the pump-laser pulses at 1030 nm. As can be seen, a broad visible emission appears when P_p crosses a certain power threshold (around 1.5 MW). Beyond such a power level, one may distinguish the generation of three main spectral peaks at 650, 460, and 400 nm,

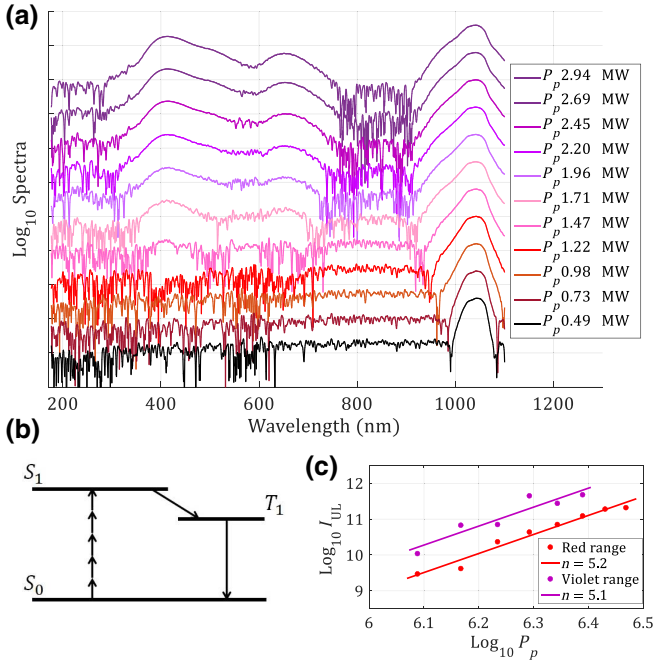

FIG. 2. (a) The UL spectra on a $\log_{10}$ scale when varying the input peak power. (b) A sketch of a five-photon-absorption UL mechanism. (c) A $\log_{10} - \log_{10}$ plot of the UL intensity as a function of the input-beam peak power. The experimental data (circles) are fitted by solid lines, the slope n of which is indicated in the legend.

respectively. Another peak, at 345 nm, can be observed at the highest input powers. The latter, which has a rather narrow bandwidth, can be easily identified with the third harmonic of the pump laser. On the other hand, we may attribute the origin of the red peak at 650 nm to the presence of NBOHCs, whereas the peaks at 460 and 400 nm can be ascribed to Ge-ODC. All of these peaks result from MPA of the pump source. We do not observe any luminescence peak at 240 nm, since it is negligible at room temperature [24].

A sketch of the MPA process involving $n = 5$ photons is shown in Fig. 2(b). Owing to MPA, an electron is excited into a higher energy band ($S_0 \rightarrow S_1$). Next, electron-phonon scattering allows the system to relax into an intermediate energy level, from which luminescence takes place, thus bringing the electron back to its ground state ($T_1 \rightarrow S_0$). The only constraint in this simple picture is that the number of photons involved must be large enough to bring the electron to its upper level. One may also note that a smaller number of photons would be required for the $S_0 \rightarrow T_1$ transition. Nevertheless, the contribution of this transition to multiphoton absorption turns out to be negligible for NBOHC and Ge-ODC defects. Theoretically forbidden for symmetry reasons, its associated oscillation strength is, in fact, one million times smaller than the $S_0 \rightarrow S_1$ transition at room temperature [25]. Therefore, as a first approximation, we may only consider the presence of the n-photon absorption process. In this simplified model, the parameter n represents the effective number of photons involved in the MPA process, since it includes all the possible contributions that we are not explicitly taking into account. We may also assume that the up-conversion rate is small enough so that the following relationship holds between the UL intensity (I_{UL}) and the nth power of P_p [26]:

$$I_{\mathrm{UL}} = \alpha P_p^n, \tag{1}$$

where the parameter α includes the n-photon absorption cross section and the phase-matching condition between the laser pump and the luminescence radiation. In this sense, it worth noting that the latter is isotropic, while the pump is mostly guided into the fiber core. Interestingly, the absorption bands corresponding to the NBOHCs and ODCs are quite close in energy. The first occurs at 258 nm and the second at 241 nm [25]. Hence, the UL generated by both defects is triggered by the same number of absorbed photons (specifically, $n = 5$ for a pump wave at $\lambda = 1030$ nm).

To confirm this, in Fig. 2(c), we illustrate the dependence of I_{UL} [calculated as the integral of the corresponding spectral peak, as shown in Fig. 2(a)] on P_p. Because of the overlap of the two ODC peaks at 400 and 460 nm, we integrate them as if they were a single signal. Figure 2(c) shows that the two fitting curves in the $\log_{10} - \log_{10}$ plot are parallel lines with a slope equal to 5, thus confirming the prediction of the simple model of Eq. (1).

The estimation of the number of photons involved in the multiphoton absorption process allows us to properly model the intensity variation of the UL along the propagation distance. The periodicity of the latter in GRIN fibers has already been pointed out as a result of the spatial self-imaging effect [18,22,27]. Nevertheless, the amplitude of the UL intensity variation along the propagation distance in a GRIN fiber could be quantitatively reproduced.

In Figs. 3(a) and 3(b), we report a microscope image of the UL scattered over the first centimeter of the GRIN fiber and its corresponding fluence variation with distance. This is obtained by a normalization of the image intensity for each pixel of propagation. The presence of a slow oscillation of the amplitude of the UL peaks, the first maximum of which occurs at about 3.5 mm, is highlighted by the solid line, which is drawn as a guide to the eye. Here, the fiber length is limited to 10 mm: after that, the metallic fiber holder introduces additional light scattering, which masks quantitative studies of the UL intensity. However, by employing longer samples, one notes a rapid quenching of visible light emission after the first few centimeters of fiber.

To further check the relation (1) between the UL and MPA, we perform a numerical simulation of spatiotemporal beam propagation in the fiber. We use a scalar 3D + 1

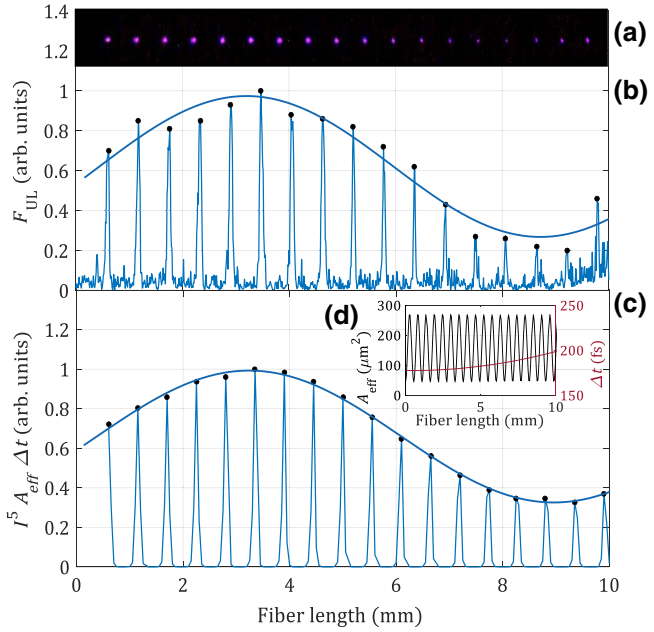

FIG. 3. (a) A digital microscope image of light scattered from the GRIN fiber, showing periodic UL emission over the first centimeter. (b) A one-dimensional (1D) plot of the corresponding integrated normalized scattered intensity versus the propagation distance. The solid line is the envelope trend of the UL peaks (black dots) along with the fiber. (c) A 1D plot of the simulated UL fluence and its envelope. (d) The simulated-beam effective area (black) and pulse duration (red) as a function of the fiber length.

GNLS equation including second-, third-, and fourth-order dispersion, Kerr, and Raman nonlinearities, as described in Ref. [21]. Random phase noise is added to the input field, in order to account for the generation of intensity speckles and seed the generation of supercontinuum and dispersive waves. Random changes in the fiber core diameter are also considered, although their effect is negligible here because of the short fiber length. Theoretically, in the case of $n = 5$ photon absorption, the UL fluence F_{UL} is related to the effective area A_{eff} and pulse duration Δt of the propagating laser beam, through the formula:

$$F_{\mathrm{UL}} \propto I^5 A_{\mathrm{eff}} \Delta t = \frac{U^5}{A_{\mathrm{eff}}^4 \Delta t^4}, \tag{2}$$

where I and U are the peak intensity and the energy of pulses along the fiber, respectively. Figure 3(c) shows that there is an excellent qualitative agreement between the experiments and numerical simulations in describing the variation of the UL emission along the fiber. In Fig. 3(d), our simulations highlight the fact that the beam effective area A_{eff} rapidly oscillates with a constant amplitude along the propagation distance, because of SSI, whereas the pulse duration Δt evolves over distances much longer than the SSI period. This means that the slow modulation of the

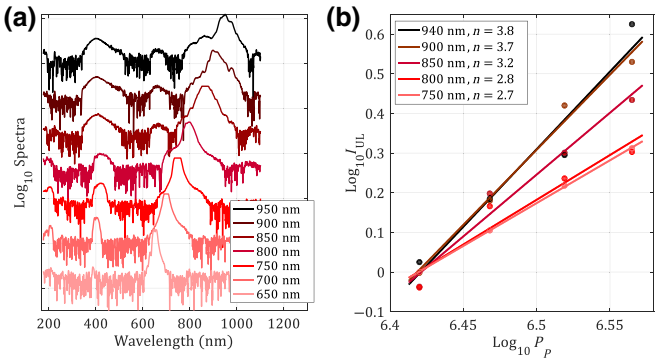

FIG. 4. (a) UL spectra, on a $\log_{10}$ scale, when the pump wavelength varies between 650 and 940 nm. (b) A $\log_{10} - \log_{10}$ plot of the UL intensity versus the pump wavelength. The experimental data (circles) are fitted by solid lines, the slope n of which appears in the legend.

UL emission in Figs. 3(a)–3(c) is due to temporal pulse reshaping or broadening. In fact, the effective area is a time-independent quantity, calculated as

$$A_{\mathrm{eff}} = \frac{\left\{\int dxdy \left[\int dt |E|(x,y,z,t)\right]^2\right\}^2}{\int dxdy \left[\int dt |E|(x,y,z,t)\right]^4}. \tag{3}$$

In order to further assess the validity of our model, we vary the pump wavelength by using the OPA. In this way, the number of photons involved in the MPA process is also varied. We tune the laser wavelength from 650 to 940 nm. In Fig. 4(a), we illustrate the variation of the UL spectrum with the pump-laser wavelength, when the input peak power is kept constant at 2.2 MW. The Ge-ODC spectral peaks at 400 and 460 nm are present and clearly visible for pump wavelengths above 750 nm.

In Fig. 4(b), we plot the Ge-ODC UL intensity as a function of the input peak power. We avoid referring to the NBOHC luminescence at 650 nm, since it is partially covered by the spectral broadening of the source. Again, the linear trend in the $\log_{10} - \log_{10}$ plots of Fig. 4(b) allows us to estimate the average number of photons that are involved in the absorption, as reported in the legend. As can be seen, the average number of photons is reduced with respect to the previous case of Fig. 2(c): here, n ranges between 3.8 and 2.7 when the pump is swept from 940 to 750 nm. These values are in agreement with the predictions of our model. Indeed, we expect the number of photons to decrease to $n = 3$ for $\lambda = 750$ nm, in order to match with the Ge-ODC absorption bands. Again, the discrepancy between theoretical and experimental values is rather small, in spite of our approximation that absorption is due to a single multiphoton process. The monotonic decrease of n as the laser wavelength is reduced clearly indicates the MPA nature of the observed UL.

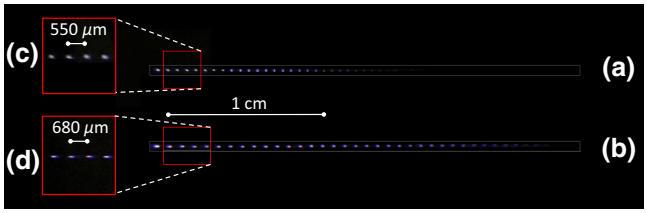

FIG. 5. (a) The UL emission from a 50-μm-core-diameter GRIN fiber with NA = 0.2. (b) The same as (a), with NA = 0.275 and core diameter of 62.5 μm. (c),(d) Enlargements of (a) and (b), respectively.

In order to highlight the effect of the Ge-ODCs concentration on the UL energy emission, we compare two GRIN fibers with different core diameters. These fibers also have different numerical apertures (NA), which grow larger with the Ge-doping concentration. In Fig. 5, we show images of UL from either 0.2 or 0.275 NA GRIN fibers (with core diameters of 50 μm or 62.5 μm, respectively), under the same input coupling conditions. As can be seen, the UL from the larger NA fiber remains visible over a fiber length that is more than twice as long, whereas the emitted UL energy is initially higher from the smaller effective area (or NA) fiber, because of the higher beam intensity in the emitting spots. Note that because of the different core diameters, different SSI periods z_p result in the two fibers, according to the law [18] $z_p = \pi r_c/\sqrt{2\Delta}$, where r_c is the core radius and Δ is the core-cladding index difference. Because of the dependence of the SSI period on the core radius, by measuring the periodicity of the UL emission one can use GRIN fibers as sensors, in order to reveal the presence of any kind of force that may introduce a variation of the core size (e.g., mechanical or thermal stress).

We also compare the UL emission of GRIN and step-index MMFs [see Fig. 1(b)]. A typical side-scattered spectrum obtained from a step-index fiber is reported as a black solid curve in Fig. 6. For ease of comparison, we also display, as a green solid curve, the UL spectrum obtained at the same power from a GRIN fiber, as in Fig. 2(a). Both spectra are normalized to the same intensity value at 650 nm. In this way, we can appreciate that the contribution of NBOHCs is much lower in a step-index fiber, since its spectral component at 1030 nm is higher (here, its peak value is cut by the saturation of the spectrometer) than that from the GRIN fiber. We can attribute this to the absence of spatial self-imaging, which increases the number of emitting spots and, as a consequence, the total contribution of NBOHC defects to the scattered light. As far as the ODCs are concerned, the UL signal is much less intense in a step-index fiber than in a GRIN fiber. This can be attributed to the lack of extrinsic Ge atoms. Nevertheless, one can still easily recognize the presence of two peaks, which are slightly shifted with respect their respective positions for the GRIN fiber. We believe that these peaks are due to intrinsic Ge impurities that are present in small amounts even in undoped commercial optical fibers [28]. However, it worth noting that Si-ODCs and Ge-ODCs have almost overlapping emission spectra and comparable oscillation strengths [25]. Therefore, UL between 400 and 500 nm in the step-index fiber may also contain a contribution from Si-associated defects.

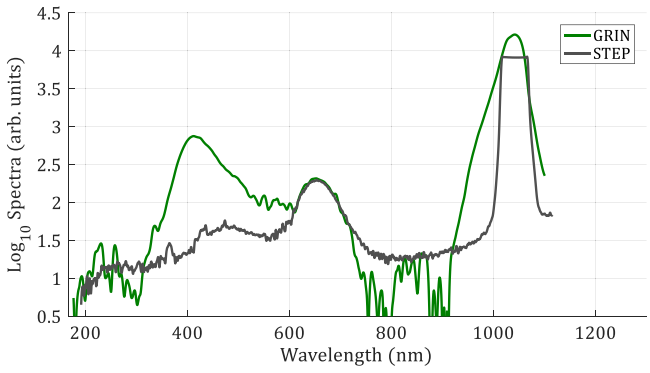

FIG. 6. A comparison of UL side-scattered spectra from either GRIN or step-index fibers, when the input peak power at 1030 nm is 2.2 MW. The curves, plotted on a $\log_{10}$ scale, are normalized to the same intensity value at 650 nm.

IV. CONCLUSION

In conclusion, we report the observation of MPA-excited UL in commercial multimode optical fibers. Based on our measurements, we estimate that MPA involving an average number of up to $n = 5$ photons is at the origin of the observed UL, in agreement with the expected position of the absorption bands. We can also directly relate the observed variation of the side-scattered UL light intensity in GRIN fibers with the simulated variation of the MPA strength along the fiber. In perspective, UL can be exploited for extending the bandwidth of supercontinuum generation into the UV frequency range. Moreover, the appearance of UL provides a useful tool to directly monitor the presence of nonlinear losses, at peak powers close to the damage threshold of optical fibers. We anticipate that our results will be of value across the range of widespread scientific and technological applications of optical fibers—e.g., in high-power fiber lasers—that will provide the next generation of particle accelerators, in nonlinear multiphoton microscopy and endoscopy, and in laser ablation and micromachining, to name a few.

ACKNOWLEDGMENTS

We acknowledge support from the European Research Council (ERC) under the European Union's Horizon 2020 research and innovation program (Grants No. 740355 and No. 874596) and the Russian Ministry of Science and Education (Grant No. 14.Y26.31.0017).

[1] F. Varsanyi and G. H. Dieke, Ion-Pair Resonance Mechanism of Energy Transfer in Rare Earth Crystal Fluorescence, Phys. Rev. Lett. **7**, 442 (1961).

[2] M.-K. Tsang, G. Bai, and J. Hao, Stimuli responsive upconversion luminescence nanomaterials and films for various applications, Chem. Soc. Rev. **44**, 1585 (2015).

[3] J. Yao, C. Huang, C. Liu, and M. Yang, Upconversion luminescence nanomaterials: A versatile platform for imaging, sensing, and therapy, Talanta **208**, 120157 (2020).

[4] S. A. Pollack, D. B. Chang, and N. L. Moise, Upconversion-pumped infrared erbium laser, J. Appl. Phys. **60**, 4077 (1986).

[5] L. F. Johnson and H. J. Guggenheim, Infrared-pumped visible laser, Appl. Phys. Lett. **19**, 44 (1971).

[6] H. You and M. Nogami, Three-photon-excited fluorescence of Al_2O_3-SiO_2 glass containing Eu^{3+} ions by femtosecond laser irradiation, Appl. Phys. Lett. **84**, 2076 (2004).

[7] H. You, T. Hayakawa, and M. Nogami, Upconversion luminescence of Al_2O_3-SiO_2:Ce^{3+} glass by femtosecond laser irradiation, Appl. Phys. Lett. **85**, 3432 (2004).

[8] X. Meng, K. Tanaka, S. Murai, K. Fujita, K. Miura, and K. Hirao, Two-photon-excited fluorescence from silicate glass containing tantalum ions pumped by a near-infrared femtosecond pulsed laser, Opt. Lett. **31**, 2867 (2006).

[9] P. G. Kazansky, H. Inouye, T. Mitsuyu, K. Miura, J. Qiu, K. Hirao, and F. Starrost, Anomalous Anisotropic Light Scattering in Ge-Doped Silica Glass, Phys. Rev. Lett. **82**, 2199 (1999).

[10] L. Skuja, The origin of the intrinsic 1.9 eV luminescence band in glassy SiO_2, J. Non-Cryst. Solids **179**, 51 (1994).

[11] L. Skuja, Optically active oxygen-deficiency-related centers in amorphous silicon dioxide, J. Non-Cryst. Solids **239**, 16 (1998).

[12] M. Cannas and F. Messina, Bleaching of optical activity induced by UV laser exposure in natural silica, J. Non-Cryst. Solids **345–346**, 433 (2004).

[13] F. Messina, F. Comandè, and M. Cannas, Effects induced by 4.7 eV UV laser irradiation on pure silica core multimode optical fibers investigated by *in situ* optical absorption measurements, J. Non-Cryst. Solids **357**, 1985 (2011).

[14] M. Kristensen, Ultraviolet-light-induced processes in germanium-doped silica, Phys. Rev. B **64**, 144201 (2001).

[15] M. Gallagher and U. Osterberg, Time resolved 3.10 eV luminescence in germanium-doped silica glass, Appl. Phys. Lett. **63**, 2987 (1993).

[16] C. Hnatovsky, D. Grobnic, and S. J. Mihailov, Nonlinear photoluminescence imaging applied to femtosecond laser manufacturing of fiber Bragg gratings, Opt. Express **25**, 14247 (2017).

[17] D. Kudarauskas, G. Tamosauskas, M. Vengris, and A. Dubietis, Filament-induced luminescence and supercontinuum generation in undoped, Yb-doped, and Nd-doped YAG crystals, Appl. Phys. Lett. **112**, 041103 (2018).

[18] K. Krupa, A. Tonello, A. Barthélémy, T. Mansuryan, V. Couderc, G. Millot, P. Grelu, D. Modotto, S. A. Babin, and S. Wabnitz, Multimode nonlinear fiber optics, a spatiotemporal avenue, APL Photonics **4**, 110901 (2019).

[19] L. G. Wright, S. Wabnitz, D. N. Christodoulìdes, and F. W. Wise, Ultrabroadband Dispersive Radiation by Spatiotemporal Oscillation of Multimode Waves, Phys. Rev. Lett. **115**, 223902 (2015).

[20] L. G. Wright, D. N. Christodoulìdes, and F. W. Wise, Controllable spatiotemporal nonlinear effects in multimode fibres, Nat. Photonics **9**, 306 (2015).

[21] M. Zitelli, F. Mangini, M. Ferraro, A. Niang, D. Kharenko, and S. Wabnitz, High-energy soliton fission dynamics in multimode GRIN fiber, Opt. Express **28**, 20473 (2020).

[22] T. Hansson, A. Tonello, T. Mansuryan, F. Mangini, M. Zitelli, M. Ferraro, A. Niang, R. Crescenzi, S. Wabnitz, and V. Couderc, Nonlinear beam self-imaging and self-focusing dynamics in a GRIN multimode optical fiber: Theory and experiments, Opt. Express **28**, 24005 (2020).

[23] L. G. Wright, D. N. Christodoulìdes, and F. W. Wise, Spatiotemporal mode-locking in multimode fiber lasers, Science **358**, 94 (2017).

[24] M. Leone, S. Agnello, R. Boscaino, M. Cannas, and F. M. Gelardi, Conformational disorder in vitreous systems probed by photoluminescence activity in SiO_2, Phys. Rev. B **60**, 11475 (1999).

[25] S. Girard, A. Alessi, N. Richard, L. Martin-Samos, V. De Michele, L. Giacomazzi, S. Agnello, D. D. Francesca, A. Morana, B. Winkler, I. Reghioua, P. Paillet, M. Cannas, T. Robin, A. Boukenter, and Y. Ouerdane, Overview of radiation induced point defects in silica-based optical fibers, Rev. Phys. **4**, 100032 (2019).

[26] M. Pollnau, D. R. Gamelin, S. R. Lüthi, H. U. Güdel, and M. P. Hehlen, Power dependence of upconversion luminescence in lanthanide and transition-metal-ion systems, Phys. Rev. B **61**, 3337 (2000).

[27] M. Karlsson, D. Anderson, and M. Desaix, Dynamics of self-focusing and self-phase modulation in a parabolic index optical fiber, Opt. Lett. **17**, 22 (1992).

[28] F. Messina, M. Cannas, and R. Boscaino, Generation of defects in amorphous SiO_2 assisted by two-step absorption on impurity sites, J. Phys.: Condens. Matter **20**, 275210 (2008).